Lasers in Manufacturing Conference 2021

Real-time adaptation of the dross attachment level in the laser cutting process based on process emission images

Matteo Pacher[a,*], Mara Tanelli[b, d], Silvia Strada[b], Davide Gandolfi[a], Sergio M. Savaresi[b] and Barbara Previtali[c]

[a]*Adige SpA, BLM GROUP, via per Barco 11, 38056 Levico T. (TN), Italy*
[b]*Dipartimento di Elettronica, Informazione e Bioingegneria, Politecnico di Milano, via G. Ponzio 34/5, 20133 Milano, Italy*
[c]*Dipartimento di Meccanica, Politecnico di Milano, via La Masa 1, 20156 Milano, Italy*
[d]*Istituto di Elettronica e Ingegneria dell'Informazione e delle Telecomunicazioni—IEIIT CNR, Corso Duca degli Abruzzi 24, 10129 Torino, Italy*

Abstract

In the field of melt and blow metal laser cutting, dross attachment is the most important quality indicator. Accordingly, process parameters are generally optimized to ensure high productivity while minimizing the level of dross attachment. The resulting set of parameters often penalizes the productivity to increase reliability. As a result, there exists a productivity margin that could be exploited by controlling the quality level in closed-loop, thus optimizing the process parameters in real-time. To closed-loop control the process, two steps must be performed: a real-time, reliable estimate of cutting quality must be available and, a closed-loop controller should adapt the process parameters according to the desired quality level. This work presents the design and experimental validation of a real-time estimation and control algorithm based on process emission images that adapts the cutting speed to fulfill a desired dross attachment level.
Project Name: LT4.0. Funding from LP6/99 Autonomous Province of Trento

Keywords: laser cutting; dross attachment; monitoring and control; camera monitoring; process emission

* Corresponding author. Tel.: +39-0461-729000; fax: +39-0461-701410.
E-mail address: matteo.pacher@blmgroup.it.

1. Introduction

In the context of metal cutting, the laser cutting technology has become the leading one mainly due to higher flexibility and enhanced productivity it offers compared to other competitive technologies. Furthermore, considering the laser-based manufacturing processes, laser cutting has the prevalent position, with revenues that amount to approximately 41% of the total laser sources market (Belforte, 2021)

In real-life industrial scenarios, both oxidation and fusion cutting modes are widely adopted; however, fusion cutting is day by day outpacing oxidation cutting thanks to the increasing laser power availability and its advantages. Indeed, fusion cutting offers a high productivity gain for low-thick materials and permits to cut a wider range of materials even if it requires a higher laser power.

The optimal process parameters are usually found via empirical modeling; this procedure is carried out in well controlled and standard conditions and yields a process behavioral model that is used to set process parameters according to specific factors such as material type and thickness. During the process, the set of parameters is accordingly mainly constant. In addition, since there exist many uncontrollable factors that affect real industrial environments, the set of process parameters is usually precautionary. Eventually, this leads to a margin either in productivity or in process quality, that could be exploited for specific manufacturing needs since conservative parameters are safer but decrease productivity.

In this context, the development of an adaptive control able to optimize the process parameters according to a specific desired quality would be beneficial both for robustness and productivity. Accordingly, the presented study focuses on the design of an adaptive control system for the fusion cutting process that adapts the cutting speed given a desired level of quality of the process. The quality of the laser cutting process is traditionally composed by many different features, namely, dross attachment, kerf width, surface roughness, heat affected zone and presence of burns on the cut edge (Caristan, 2004). Nevertheless, among all these features dross attachment plays the most important role (Goppold et al., 2016; Pacher et al., 2017; Thombansen et al., 2014). As a consequence, this work considers dross attachment only as quality parameter and proposes a continuous indicator to map the appearance of significant dross levels in real-time.

In the literature, several contributions studies the monitoring and control of the laser cutting process, see e.g. (Adelmann et al., 2016; De Keuster et al., 2006; Decker et al., 1997; Duflou et al., 2009; H. Jørgensen, 1991; Kaebernick et al., 1998; Levichev et al., 2021, 2020; Sforza et al., 1997; Sichani et al., 2010). Among others, a dross attachment detection algorithm has been presented by Schleier et al., 2017 where photodiodes were used as source of information. Focusing to camera-based monitoring, Levichev et al., 2021 recently proposed a study where the dross attachment in fusion cutting seems to be correlated to the standard deviation of intensity and other factors of the process emission shape. In addition, Pacher et al., 2020 and Franceschetti et al., 2020 presented two novel approaches based on image processing, machine learning and deep learning techniques to estimate the dross attachment accurately and in real-time based on process emission images. Finally, to date only few contributions presenting the feedback control of the laser cutting process exists. These contributions (Duflou et al., 2009; Sichani et al., 2010) however focus on oxidation cutting only.

In this study, an innovative continuous indicator of dross attachment is used as quality indicator of the laser cutting process. This dross attachment indicator is estimated via the real-time elaboration of process emission images coupled with machine learning techniques. Finally, a controller that adapts the cutting speed to track the desired level of dross attachment was designed and closed-loop experiments were performed to validate the entire processing and actuation chain.

2. Experimental setup

The cutting experiments were carried out using a BLM GROUP LC5 machine equipped with an IPG YLS-6000 laser source; the maximum available power is of 6kW and the transport fiber diameter is equal to 100µm. The laser cutting head is a Precitec HP SSL mounting having collimation and focal lenses of 100mm and 200mm, respectively. The laser spot diameter in the waist is therefore equal to 200µm.

To measure the dross attachment of the specimens, images of the cut edges were collected using an echo-LAB SM 535 H microscope by Devco Srl having a resolution of 5µm/px and a field of view of 230x170mm.

To monitor the laser cutting process, a custom monitoring chain was designed, and the laser head was adapted to accommodate a coaxial camera setup as shown in Figure 1. The designed monitoring setup is focused on the acquisition of near infrared process emission images based on existing literature (Duflou et al., 2009; Mazzoleni et al., 2019); to this end, the process emission is filtered using a near-infrared band pass filter.

The selected sensor is an industrial CMOS camera having sensor size equal to 1280x1024px and a pixel dimension of 4.8x4.8µm. The camera lens was selected to obtain a field of view of 2x2mm and a spatial resolution of 9.6µm/px. Eventually, the selected sensor permitted to reach a high frame rate of 1500fps collecting monochrome images if size 210x210px.

A microcontroller was used to acquire the process parameters (e.g., cutting speed, laser power, etc.) at a sample rate of 10kHz and for producing a TTL signal to be used as trigger for the image acquisition; this eventually permits to perfectly synchronize images and process inputs.

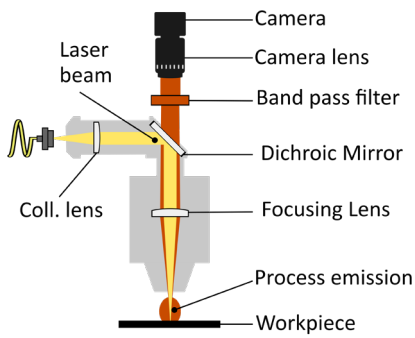

Fig. 1. Designed monitoring architecture for coaxial camera monitoring.

2.1. Structure of the experiments

During the study, several experiments have been carried out. To model the dross attachment formation through the machine learning approach described in (Pacher et al., 2020), different experiments was performed where the goal was to produce a reasonably large quality variability. During these experiments, stainless steel X5CrNi18-10 and mild steel S235JR were cut in the thickness range 3 – 10mm.

After confirming the validity of the estimation algorithm, the scope of closed-loop controlled experiments was reduced to the 3mm AISI 304 material only, since it represents the most challenging and significant processing conditions. This is due to the wider process window and to the relatively high cutting speed that requires a fast estimation and control algorithms. Accordingly, some ad-hoc experiments to fine-tune the model for 3mm material were performed. The fixed process parameters are reported in Table 1 and only the cutting speed was varied between 7000 – 9500mm/min with steps of 500 mm/min (6 exp. points, see Figure

2). For each condition three replicates were performed for a total of 18 cuts. It is emphasized that these conditions may represent an industrial process widow obtained after empirical parameter optimization.

Table 1. Fixed process parameters for 3mm model fitting experiments.

Parameter	Value
Laser Power, P	6000 W
Gas pressure, p	12 bar
Focal position, f	-2.8 mm
Standoff distance, sod	0.7 mm
Nozzle diameter, d_{nozzle}	1.8 mm

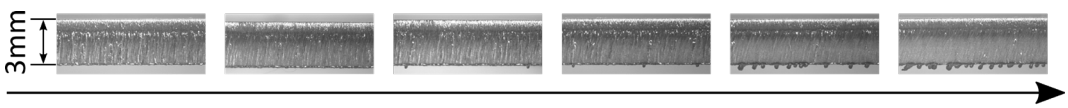

Fig. 2. View of the obtained quality variation during the 3mm ad-hoc experiment for model fitting.

After the model was estimated, closed-loop experiments were performed using 3mm X5CrNi18-10 material where the goal was to track different dross attachment conditions from dross-free to high-dross.

3. Real-time dross estimation

This section outlines how the real-time dross attachment estimation is performed.

3.1. Definition of the dross attachment indicator

A quantitative measure of dross attachment is fundamental for the design of a real-time estimation algorithm. Indeed, during the fitting phase of a model, there is the need to quantitatively map parameters obtained from the monitoring chain to variables representing the amount of the produced dross attachment.

The dross attachment indicator is designed to be a continuous, normalized, dimensionless and bounded quantity that describes the amount of *significant* dross attachment within a given time interval. The term *significant* indicates that this indicator aims at tolerating the dross attachment that falls below a given threshold therefore focusing on the perceived dross attachment. The threshold has been finely tuned according to the expertise of skilled technicians.

The dross attachment indicator is build considering the dross attachment profile along the full specimen geometry. This dross profile is measured via image processing algorithms that at first stitches three subsequent images of the specimen side, align the resulting image according to the upper side of the specimen side and finally extracts the thickness profile, T, thanks to well-known gradient based techniques. An example of the application of the algorithm is given in Figure 3.

The dross attachment profile, h, is then obtained subtracting the sheet thickness, T_n, from the total thickness as a function of the linear abscissa, d, as

$$h(d) = T(d) - T_n \,. \qquad (1)$$

Considering the displacement profile available from the recorded process inputs, the latter displacement-based quantity can be remapped in the time domain as

$$h(d(k)) = h(k), \tag{2}$$

where k is the discrete-time abscissa $k = i\Delta t, i \in \mathbb{N}$ being Δt the sampling period. Finally, $h(k)$ has been squared to emphasize the dross droplets with respect to the baseline. After the measurement and preliminary manipulation of the dross attachment profile, the information of significant dross height, h_0^2, is introduced and the squared profile is binarized as follows:

$$h_{th}^2(k) = \begin{cases} 1 & h^2 > h_0^2, k \geq 0 \\ 0 & otherwise \end{cases}, \tag{3}$$

where the value of h_0^2 is equal to 0.03mm^2. The latter quantity is dimensionless and bounded and since it is binary it is a good candidate to train classification models. To obtain a continuous indicator, h_{th}^2 is averaged using the moving average operator as

$$y(k) = \frac{1}{\gamma + 1} \sum_{j=0}^{\gamma} h_{th}^2(k - j), \tag{4}$$

where γ is the size of the look-back window. This latter quantity represents the selected quantitative dross indicator that will be estimated and controlled in real-time.

3.2. Estimation of the dross attachment indicator

The estimation of $y(k)$ is based on the analysis of process emission images collected by a coaxial camera filtered in the near infrared wavelength range. The estimation is constituted of two parts: *featuring* and *mapping*. Generally speaking the featuring part consists in synthetizing the information contained in raw data into a compact set of features whereas in the mapping part, a model is fit between inputs and outputs.

In this work, the featuring part contains the following operations:

1. image processing of raw images to extract geometrical indicators of the laser irradiated zone;
2. pre-processing of the geometrical features in the time domain;
3. pre-processing of features obtained at step 2. In the probabilistic domain.

The image processing algorithm binarizes the process emission images and computes the average intensity, I, the length, l, and width, w, of the binarized image. The extracted geometrical features are visualized in Figure 3.

These features are combined in the second step to produce other candidate features such as the form factor of the process image, w/l. Finally, standard probabilistic indicators i.e. the mean, the variance and the skewness corresponding to the first three central moments of a distribution have been considered for the last featuring step. These three probabilistic indicators have been computed for each time signal using the data contained in the look-back moving window γ as for $y(k)$.

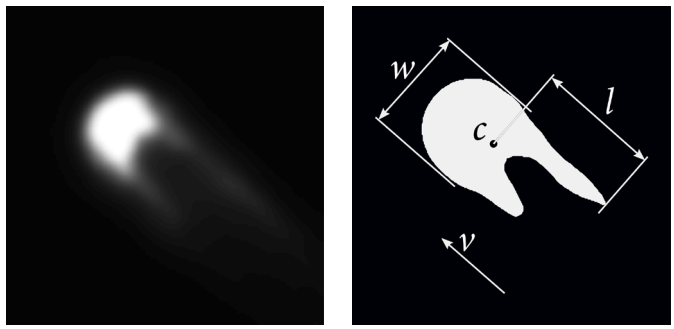

(a) (b)

Fig. 3. Example of the image analysis algorithm applied to a process emission image (a) to extract geometrical features (b).

At the end of the featuring step, several features have been computed. However, to avoid overfitting, only three features have been used iteratively as model inputs; considering the fitting results in terms of model accuracy, the three most informative features have been selected and the final model have been fit.

The model structure has been kept constant during the mapping phase to a standard fully connected neural network having a single hidden layer composed by N_{neur} neurons.

As a result, the three most informative features for the data of the experiments focused on the 3mm thickness only are the mean values of the image intensity, length and width of the laser irradiated zone. After the feature selection iterative procedure, sensitivity analysis has been carried out to determine the numerical parameters of the model, i.e., the number of neurons and the length of the lookback window and the two values were fixed to 5 and 100ms, respectively. Thanks to the high frame rate of the camera, the obtained model relies on 25000 data points.

The results of the real-time estimation algorithm are shown in Figure 4. The total computational time for the featuring and mapping phase has been measured equal to 0.3ms for the single frame (compiled code running on a Dell XPS equipped with an Intel i7 processor) thus making the real-time estimation feasible for the target acquisition rate of 1500fps that corresponds to a sampling period is equal to 0.67ms.

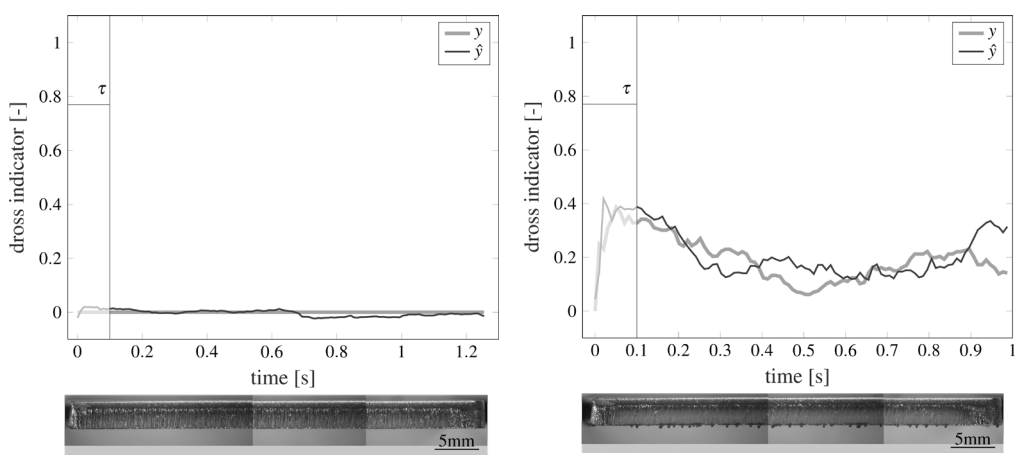

(a) (b)

Fig. 4. Results if the dross attachment estimation algorithm for dross-free (a) and intermediate dross (b) conditions. Cutting speed equal to 7000mm/min (a) and 8500mm/min(b), other process parameters contained in Table 1.

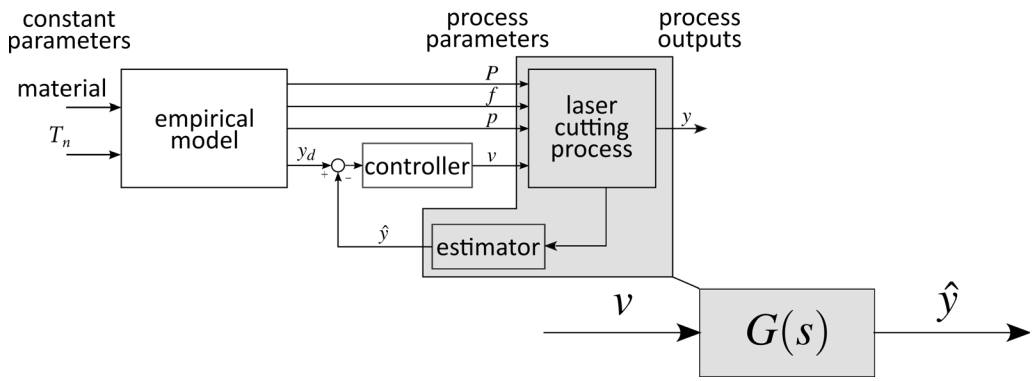

Fig. 3. Block diagram of the controlled system composed by the laser cutting process and the estimator developed in Section 3.

4. Identification of the process dynamics and control design

4.1. Identification experiments setup

As previously described, the target is to control the amount of produce dross attachment by adapting the cutting speed. Accordingly, the identification of the system composed by the process and the estimator dynamics has been performed (see Figure 5). In other words, the transfer function $G(s)$, linking the input v and the output y has been estimated via the frequency-domain parametric identification approach.

In principle, a control algorithm could potentially run at a really high sampling rate. In fact, after a time equal to the look-back window, i.e., 100ms, the output estimate is available at the same sampling rate of the camera, hence at 1500fps. However, because of the analog connections between the different components of the system the bandwidth of the full actuation chain has been measured to be only of 7.5Hz, probably due to limitations in the analog to digital conversion of the control input. This poses noticeably limitations to the achievable closed-loop response time and to the frequency range for system identification. Due to this limitations, the desired bandwidth of the controlled system has been set to 1Hz. Ongoing work is focused at enhancing the overall performance to reach a bandwidth of approximately 100Hz, which is in principle achievable with an improved experimental setup.

Due to the frequency limitations, the identification experiments are performed in the 0.75–3Hz frequency range with steps of 0.25Hz cutting along a straight line of length 400mm of 3mm X5CrNi18-10 stainless steel. Process parameters are set according to previous experiments and the cutting speed is varied according to a sinusoidal wave to excite the system at a given frequency. The variation range of the cutting speed has been set from 6800 to 9700mm/min. This speed range proved to produce dross-free to high dross cuts in the considered experiments.

4.2. System identification

Using the points of the experimental frequency response derived from data (see Figure 6), a first order dynamical system with delay proved accurate enough to describe the overall system, at least within the tested frequency range. The system model is thus

$$G(s) = \frac{\mu_G}{1 + s\,T_G} e^{s\tau_G}, \tag{5}$$

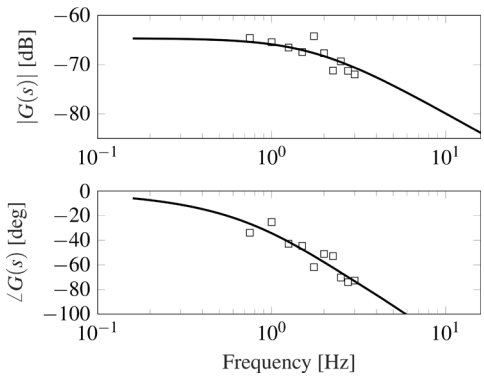

Figure 4. Results of the experimental identification of the system dynamics via the frequency-domain parametric identification method.

where the parameters are μ_G, T_G and τ_G representing the static gain, the time constant and the pure delay, respectively. Given the very fast process dynamics, the pole and the static delay in the model are probably due to the estimator dynamics, which introduces low-pass filtering effects. In fact, the pure cutting phase should induce a dynamic response in the order of hundreds of Hertz due to the high-rate at which the material is melted by the laser beam, so outside the range currently analyzed in the experiments, and anyway much beyond the needed closed-loop bandwidth. A more thorough analysis of the two distinct dynamics will be carried out when higher-frequency excitation tests will be possible.

4.3. Control design

A simple proportional controller $R(s) = K$ was selected to demonstrate the possibility of a feedback approach. This choice is motivated by the frequency limitations and the given system dynamics.

The value of the proportional gain is initially estimated as $K = 1800$ to meet the requirement of 1Hz of bandwidth of the loop transfer function

$$L(s) = R(s)G(s) = K\frac{\mu_G}{1 + s\,T_G}e^{s\tau_G}. \qquad (6)$$

A saturation block is introduced in in cascade to the controller to avoid unfeasible speed settings. Control experiments are carried out to validate the capabilities of the presented methodology. The cut geometry is the same as for the identification experiments, i.e., a straight line of length 400mm.

5. Closed-loop experimental results

During the experiments different set points in terms of desired dross attachment, y_d, are commanded to the controller to investigate the capabilities of the controller in following an arbitrary quality requirement. The initial cutting speed (initial condition) is set according to the set point to see the effect of the controlled adaptation. For instance, for a mid-high value of the set point, the initial speed is set to have a dross-free cut. Conversely, for dross-free set point value, the initial cutting speed is set to obtain a high-dross cut.

Figure 7 show three examples of feedback-controlled cuts. It is observed that in all conditions the controller reaches the setpoint (even if some oscillations occur) and then maintains the desired level of dross attachment till the end of the cut.

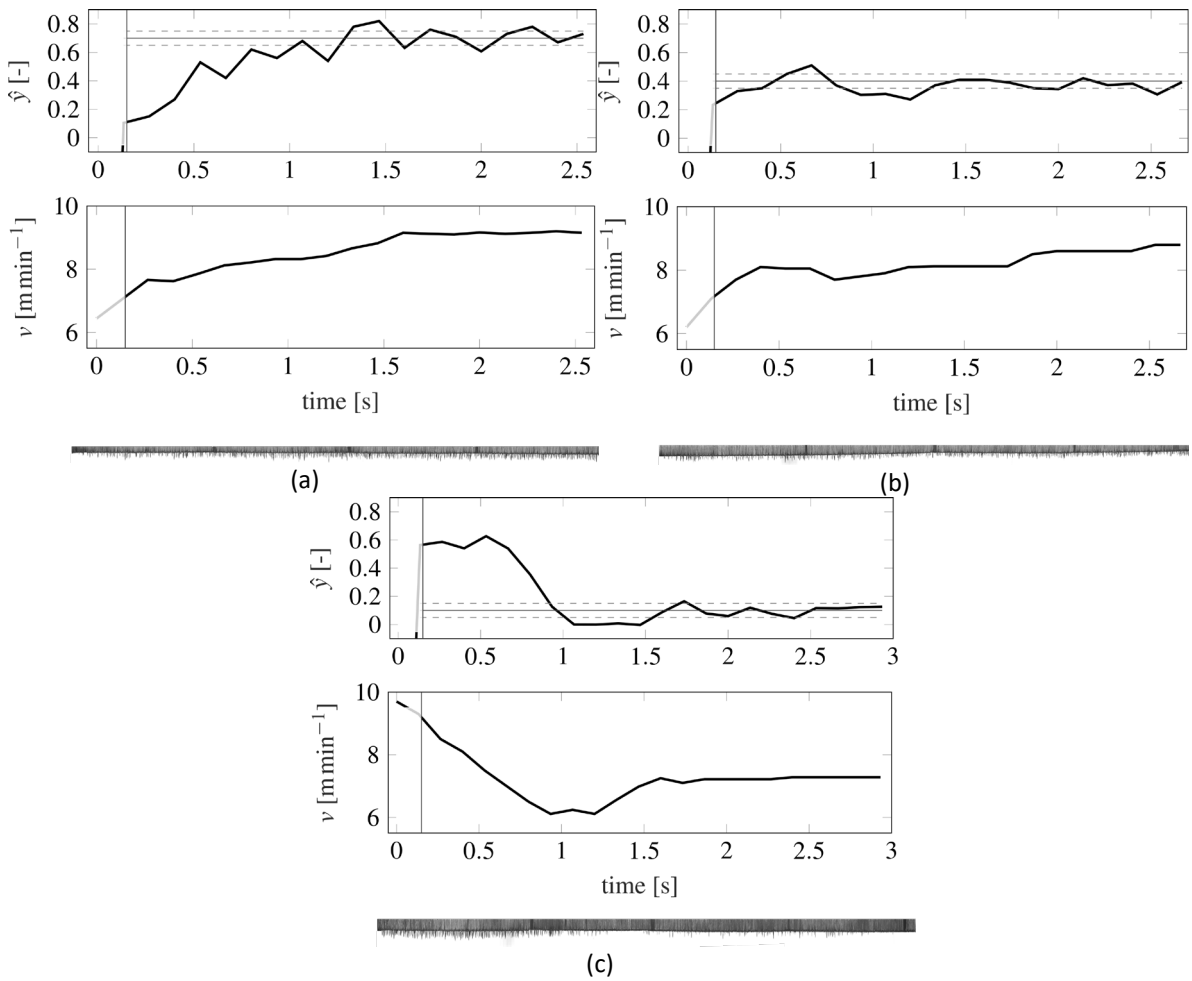

Fig. 7. Results of the closed-loop controlled experiments for high-dross (a), intermediate dross (b) and dross-free (c) setpoints.

6. Conclusion

This paper presented the complete implementation of a closed-loop control system for adapting the cutting speed to produce the desired level of quality in terms of amount of dross attachment. A real-time advanced estimation of the controlled variable has been demonstrated, based on fast processing of process emission images collected by a coaxial camera installed on the laser head. Future works will focus at enhancing the existing hardware setup in order to obtain higher sampling frequencies, which will enable a more extensive testing of the overall closed-loop system.

Acknowledgements

The authors gratefully acknowledge Adige SpA for the great cooperation and for their excellent support. The presented study has been funded with the contribution of the Autonomous Province of Trento, Italy, through the Regional Law 6/99. Name of the granted Project: LT4.0.

References

Adelmann, B., Schleier, M., Neumeier, B., Hellmann, R., 2016. Photodiode-based cutting interruption sensor for near-infrared lasers. Appl. Opt., AO 55, 1772–1778.

Belforte, D., 2021. A view of the 2020/2021 industrial laser market [WWW Document]. Industrial Laser Solutions. URL https://www.industrial-lasers.com/home/article/14196074/a-view-of-the-20202021-industrial-laser-market (accessed 5.3.21).

Caristan, C.L., 2004. Laser Cutting Guide for Manufacturing. Society of Manufacturing Engineers, Dearborn, Michigan.

De Keuster, J., Duflou, J.R., Kruth, J.P., 2006. Monitoring of high-power CO2 laser cutting by means of an acoustic microphone and photodiodes. International Journal of Advanced Manufacturing Technology 35, 115–126.

Decker, I., Heyn, H., Martinen, D., Wohlfahrt, H., 1997. Process monitoring in laser beam cutting on its way to industrial application, in: Beckmann, L.H.J.F. (Ed.), . Presented at the Lasers and Optics in Manufacturing III, Munich, Germany, pp. 29–37.

Duflou, J.R., Sichani, E.F., Keuster, J.D., Kruth, J.-P., 2009. Development of a real time monitoring and adaptive control system for laser flame cutting. ICALEO 2009, 527–536.

Franceschetti, L., Pacher, M., Tanelli, M., Strada, S.C., Previtali, B., Savaresi, S.M., 2020. Dross attachment estimation in the laser-cutting process via Convolutional Neural Networks (CNN), in: 2020 28th Mediterranean Conference on Control and Automation (MED). Presented at the 2020 28th Mediterranean Conference on Control and Automation (MED), pp. 850–855.

Goppold, C., Pinder, T., Herwig, P., 2016. Transient beam oscillation with a highly dynamic scanner for laser beam fusion cutting. Advanced Optical Technologies 5, 61–70.

H. Jørgensen, F.O.O., 1991. Process monitoring during CO2 laser cutting, in: Proceedings Volume 1412, Gas and Metal Vapor Lasers and Applications. Presented at the Optics, Electro-Optics, and Laser Applications in Science and Engineering, Los Angeles, CA, pp. 198–208.

Kaebernick, H., Jeromin, A., Mathew, P., 1998. Adaptive Control for Laser Cutting Using Striation Frequency Analysis. CIRP Annals - Manufacturing Technology 47, 137–140.

Levichev, N., Costa Rodrigues, G., Vorkov, V., Duflou, J.R., 2021. Coaxial camera-based monitoring of fiber laser cutting of thick plates. Optics & Laser Technology 136, 106743.

Levichev, N., Rodrigues, G.C., Duflou, J.R., 2020. Real-time monitoring of fiber laser cutting of thick plates by means of photodiodes. Procedia CIRP, 11th CIRP Conference on Photonic Technologies [LANE 2020] 94, 499–504.

Mazzoleni, L., Demir, A.G., Caprio, L., Pacher, M., Previtali, B., 2019. Real-Time Observation of Melt Pool in Selective Laser Melting: Spatial, Temporal and Wavelength Resolution Criteria. IEEE Transactions on Instrumentation and Measurement 1–1.

Pacher, M., Franceschetti, L., Strada, S.C., Tanelli, M., Savaresi, S.M., Previtali, B., 2020. Real-time continuous estimation of dross attachment in the laser cutting process based on process emission images. Journal of Laser Applications 32, 042016.

Pacher, M., Monguzzi, L., Bortolotti, L., Sbetti, M., Previtali, B., 2017. Quantitative identification of laser cutting quality relying on visual information, in: LiM 2017 Proceedings. Presented at the Lasers in Manufacturing (LiM) 2017, Munich, pp. 1–11.

Schleier, M., Adelmann, B., Neumeier, B., Hellmann, R., 2017. Burr formation detector for fiber laser cutting based on a photodiode sensor system. Optics & Laser Technology 96, 13–17.

Sforza, P., Dell'Erba, M., Santacesaria, V., de Blasiis, D., Lombardo, V., 1997. A three-modules sensor for CO2 laser welding and cutting processes, in: Proceedings Volume 3097, Lasers in Material Processing. Presented at the Lasers and Optics in Manufacturing III, Munich, pp. 97–107.

Sichani, E.F., De Keuster, J., Kruth, J.-P., Duflou, J.R., 2010. Monitoring and adaptive control of CO2 laser flame cutting. Physics Procedia, Laser Assisted Net Shape Engineering 6, Proceedings of the LANE 2010, Part 2 5, 483–492.

Thombansen, U., Hermanns, T., Stoyanov, S., 2014. Setup and maintenance of manufacturing quality in CO2 laser cutting. Procedia CIRP 20, 98–102.